Доклади на Българската академия на науките
Comptes rendus de l'Académie bulgare des Sciences
Tome 76, No 5, 2023

ENGINEERING SCIENCES
Automatics and informatics

BRAIN COMPUTER INTERFACE SYSTEM FOR UAV TARGET SEARCHING

Tian Wei Shi#, Jiao Feng Qiang, Guang Ming Chang, Ling Ren*

Received on November 9, 2022
Presented by S. Hadjitodorov, Corresponding Member of BAS, on January 31, 2023

Abstract

This paper proposes a Brain Computer Interface (BCI) system for unmanned aerial vehicle (UAV) indoor space target searching. The monocular vision navigation subsystem provides three-dimensional (3D) space feasible flight directions. To realize four-class motor imagery (MI) electroencephalogram (EEG) features extraction (left/right-hand, feet and tongue), the decision subsystem adopts a mathematical paradigm combining "one versus one" (OVO) and "one versus rest" (OVR) to traditional Common Spatial Pattern (CSP). Simultaneously, it utilizes a 2-layer hierarchical support vector machine (HSVM) to realize the feature classification and final feasible flight direction decision. The actual indoor space target searching experiment verifies that this BCI system has good adaptability.

Key words: Brain Computer Interface, Motor Imagery, electroencephalogram, Common Spatial Pattern, Hierarchical Support Vector Machine

Introduction. With the improvement of control theories, computer technologies and artificial intelligence, the unmanned aerial vehicle (UAV) has got more attention in object detection and tracking [1], indoor target searching and task scheduling [2], intelligent traffic policing and emergency response [3], etc.

#Corresponding author.

Tian Wei Shi has been supported by the Natural Science Foundation project of Liaoning Province (2021-KF-12-06), Department of Education of Liaoning Province (2020FWDF01), and Project of Liaoning BaiQianWan Talents Programme.

DOI:10.7546/CRABS.2023.05.12

BCI system can build communication channel between spontaneous brain electrical activities inspired by cerebral cortex nerve cells and external devices using electroencephalogram (EEG) signals. It can be implemented in various ways such as P300 [4], steady-state visual evoked potential (SSVEP) [5] and MI [6], etc. Since MI does not rely on external stimuli, it has better controllability and potential application prospects, such as devise control in virtual reality environment [7], mental fatigue process detection [8], hand movement direction decoding for stroke recovery and rehabilitation [9], etc. To accomplish indoor three-dimensional (3D) space target searching using UAV, Shi et al. [2] designed a Electrooculography (EOG) and EEG-based hybrid computer interface (HCI) system. This HCI system added an interface subsystem to complete horizontal and vertical MI tasks switching. They adopted Continuous Wavelet Transform (CWT) to detect continuous blinking EOG features. However, it cannot directly realize 3D flight direction selection and flight control.

To solve this problem, this paper proposes an indoor 3D space target searching BCI system with monocular vision navigation and decision subsystems for a low speed UAV. To design the monocular vision navigation subsystem, different methods can be utilized to deal with the obstacles detection and avoidance, such as building 3D obstacle model [10], calculating obstacles depth [11], and using stereo camera to implement obstacles estimation at short range [12]. These methods estimate the size and position of obstacles and calculate the distance relationship between obstacles and UAV. However, they are computationally and time-intensive. Thus, the monocular vision navigation subsystem used in Shi et al., [13] was applied. It utilizes the Scale Invariant Feature Transform (SIFT) and Brute-Force (BF) methods to extract the key points of obstacles, complete the key points matching and optimization, and supply the feasible flight directions for decision subsystem. The decision subsystem is constructed based on the analysis of MI tasks (left/right-hand, feet and tongue) EEG collected from 15 electrodes. Feature extraction is employed to get the regular patterns of brain activities from the gathered raw MI tasks EEG signals. To implement the four-class classification, a mathematical paradigm combining "one versus one" (OVO) and "one versus rest" (OVR) to the traditional Common Spatial Pattern (CSP) was used [14]. In addition, the Hierarchical Support Vector Machine (HSVM) is applied to complete feature classification.

The rest of this paper is organized as follows. The methods and experiments used in this paper are explained in Section 2. Sections 3 and 4 present the actual indoor target searching experimental results and discussions. Section 5 describes the conclusion.

Experimental. ***MI data acquisition.*** In accordance with the international 10–20 system, the Neuroscan (NuAmps) with 40 channels Ag/AgCl electrodes is closely attached to subject's scalp. The linked ears electrodes are used as the reference. The EEG signals are stored as digital signals at 250 Hz with 22 bit by

FT7, FC3, FCZ, FC4, FT8, T3, C3, CZ, C4, T4, TP7, CP3, CPZ, CP4, and TP8 electrodes.

MI data preprocessing. Firstly, the 50 Hz notch filter is utilized to remove the power noise from the collected EEG signals. Secondly, the 3–34 Hz bandpass filter is used to eliminate the high-frequency noise. Finally, the 5-layer wavelet packet decomposition is applied to analyze the filtered EEG signal. The experimental results show that the amplitude of reconstructed EEG signal is very weak in the range of 25–34 Hz and hardly changes during the process of executing the MI tasks. Therefore, the EEG signals in 3–24 Hz frequency band are selected for MI tasks feature extraction and classification.

MI feature extraction. The OVO and OVR strategies are applied to implement feature extraction for the left-hand MI task (class 1, movement to turn left), right-hand MI task (class 2, movement to turn right), two feet MI task (class 3, movement to fly up) and tongue MI task (class 4, movement to fly down).

In OVO strategy, let $X_i \in \mathbb{R}^{T\times N}$ $(i \in \{1,2\})$ be MI task EEG signal for the reconstructed class i, N is the channel number, T is the number of time series samples per channel for a single training. Define the covariance of the single training sample for class i as:

$$C_i = \frac{X_i X_i^T}{\mathrm{trace}(X_i X_i^T)}, \tag{1}$$

where X_i^T is the transpose of X_i; $\mathrm{trace}(X_i X_i^T)$ is the sum of the elements on the matrix's main diagonal. The spatial covariance C_i is calculated by averaging all samples trained in each group. Define the composite spatial covariance C as:

$$C = C_1 + C_2 = U_0 \wedge U_0^T, \tag{2}$$

where U_0 is the eigenvector matrix; $\wedge$ is the diagonal matrix of eigenvalues in descending order. The whitening transform can be described as follows:

$$P = \wedge^{1/2} U_0^T. \tag{3}$$

The spatial covariance C_i can be redescribed as:

$$S_1 = PC_1P^T = B \wedge_1 B^T, \qquad S_2 = PC_2P^T = B \wedge_2 B^T, \tag{4}$$

where S_1 and S_2 share the eigenvectors. Since $\wedge_1 + \wedge_2 = I$, the maximum eigenvalue in S_1 corresponds to the minimum eigenvalue in S_2. The eigenvectors in B are used for the classification. When the whitened EEG signal is mapped to the first and last eigenvectors, the optimal eigenvector of the EEG signal for distinguishing two classes will be obtained. The mapping matrix and the mapping process of a training sample can be given by:

$$W_{12} = B^T P \tag{5}$$

$$Z_{12} = W_{12}X. \tag{6}$$

The rows and columns of the mapping matrix W_{12} can be considered distribution eigenvectors of EEG signals, and common space pattern, respectively. According to Eq. (6), MI features for classification can be extracted by decomposing the whitened EEG signal.

In OVR strategy, one class is defined as the target class, and the others are defined as the opposite class. The CSP is utilized to calculate the covariance and whitening transform for each training. However, the common space pattern is calculated differently:

$$C = C_1 + C_{1r}, \quad C_{1r} = C_2 + C_3 + C_4. \tag{7}$$

After the whitening transform,

$$S_{1r} = P_{1r}C_{1r}P_{1r}^T = B_{1r} \wedge_{1r} B_{1r}^T, \quad \wedge_1 + \wedge_{1r} = I. \tag{8}$$

The mapping matrix and mapping process of single training can be described as:

$$W_1 = B_{1r}^T P_{1r} \tag{9}$$

$$Z_1 = W_{1r}X. \tag{10}$$

Calculating the feature vector f_i using Eq. (11):

$$f_i = \log\left(\frac{\mathrm{VAR}_i}{\sum_{i=1}\mathrm{VAR}_i}\right) \quad , \tag{11}$$

where VAR_i represents the best-mapped variance matrix of Z_1. Finally, the obtained feature vector is expressed as:

$$f = [f_{12}, f_{13}, f_{14}, f_{23}, f_{24}, f_{34}, f_1, f_2, f_3, f_4], \tag{12}$$

wheref_{12}, f_{13}, f_{14}, f_{23}, f_{24} and f_{34} represent the extracted feature vector corresponding to OVO strategy, f_1, f_2, f_3, and f_4 represent the extracted feature vector corresponding to OVR strategy.

MI feature classification. In the HSVM method, four OVR (first layer) and six OVO (second layer) SVM classifiers are used, respectively. In the first layer classification process: 1) If only one OVR classifier obtains the valid result (the other three are invalid), this result is the final classification output result; 2) If any two OVR classifiers get the valid results (the other two are invalid), the two results are input to the corresponding OVO classifier for the second layer classification. The classification result is the final classification output; 3) If more

than two OVR classifiers acquire the valid results, the four MI tasks EEG signals are input to the six OVO classifiers for the second layer classification. If more than three OVO classifiers get the same classification result, it will be output as the final classification result.

Actual indoor target searching experiment. Experiment setup. Twelve healthy subjects (three males and three females (subjects 1–6) had participated in calibration experiment, aged 20.2 ± 1.3 years; three males and three females (subjects 7–12) had not participated in the calibration experiment, aged 20.8 ± 1.4 years, were invited to complete this experiment. Subjects attached electrode caps and sat comfortably in an armchair. The real-time video and feasible flight directions sent by UAV were displayed on the monitor in the first field of view. The searching target is hung on the "Target". Subjects do not know its position and take off UAV at "Start". This experiment consisted of one upward, two downward, one cylindrical, four rectangular obstacles, one non-flying zone and two walking people. Subjects are previously unfamiliar with the experimental environment and completed this experiment on the same day. The decision subsystem was run on DELL XPS8940 with i7-11700 CPU, RTX 3060Ti graphics card and 32 GB RAM.

UAV flight control. Subjects take off and land UAV manually. They utilize MI tasks to select corresponding feasible flight direction. If subjects select a feasible flight direction, it is set as autonomous flight direction of UAV subsequently. During this process, UAV remains hovering. If subjects do not select all feasible flight directions, they must control UAV using MI tasks (left-hand to turn left, right-hand to turn right, two feet to fly upward and tongue to fly downward) independently until next time feasible flight directions selection. The decision subsystem sends control instructions per 30 ms. If UAV does not receive any control instruction in 2 s, it will hover and wait for receiving control instruction. Once UAV encounters someone walking towards it, the UAV will retreat and re-provide feasible flight directions automatically.

Results and discussion. ***Results for actual indoor target searching experiments.*** Figure 1 a, b indicates the actual trajectories of subjects 1–12.

Table 1 illustrates the distance error (DE, mean ± S.D.), rotation error (RE, mean ± S.D.), time cost (TC) and classification accuracy (CA) results of subjects 1–12.

To verify the performance of this BCI system, this experiment is divided into two parts in accordance with the trajectories in Fig. 1(b). Table 2 describes the time cost, classification accuracy, distance errors and rotation errors results of subjects 7–12 (1 and 2 represent the first and second part, respectively).

In Figure 1, subjects 2 and 5 had cost the minimum time and MI tasks. They had the best distance and rotation errors. Since subjects did not know the position of "Target", subjects 1, 3 and 4 chose a feasible flight direction away from the "Target" at the intersection. Subjects 1–6 were able to complete the

Table 1

Results of subjects 1–12

Subjects	DE/cm	RE/°	TC/s	CA/%
1	5.97 ± 1.6	5.52 ± 1.8	217	72.08
2	5.33 ± 1.5	5.14 ± 1.7	198	80.11
3	6.26 ± 1.7	5.88 ± 1.8	235	68.01
4	6.15 ± 1.6	5.58 ± 1.8	224	69.49
5	5.54 ± 1.5	5.26 ± 1.7	206	75.25
6	5.95 ± 1.7	5.42 ± 1.7	211	71.02
7	9.57 ± 3.1	10.03 ± 3.2	324	62.34
8	9.71 ± 3.1	10.25 ± 3.2	337	60.13
9	10.16 ± 3.4	11.02 ± 3.5	361	55.17
10	9.48 ± 3.0	9.87 ± 3.1	298	65.03
11	9.79 ± 3.2	10.47 ± 3.3	315	64.27
12	9.92 ± 3.3	10.67 ± 3.4	349	57.06

Table 2

Time cost and classification accuracy comparison results for subjects 7–12

Subjects	TC1/s	TC2/s	CA1/%	CA2/%	DE1/cm	DE2/cm	RE1/°	RE2/°
7	187	137	57.66	67.02	12.11 ± 4.0	7.03 ± 1.9	12.72 ± 4.2	7.34 ± 2.0
8	190	147	55.02	65.24	12.29 ± 4.1	7.13 ± 2.0	12.95 ± 4.3	7.55 ± 2.1
9	201	160	48.80	61.54	12.82 ± 4.2	7.46 ± 2.2	13.60 ± 4.4	8.44 ± 2.2
10	176	122	60.68	69.38	12.03 ± 4.0	6.92 ± 1.9	12.53 ± 4.3	7.21 ± 2.0
11	174	141	60.41	68.13	12.43 ± 4.1	7.25 ± 2.0	13.09 ± 4.3	7.85 ± 2.1
12	193	156	50.84	63.28	12.48 ± 4.1	7.36 ± 2.1	13.30 ± 4.4	8.04 ± 2.2

feasible flight direction selection well. Because subjects 7–12 were not familiar with MI tasks or performed incorrect MI tasks, they had large distance errors and

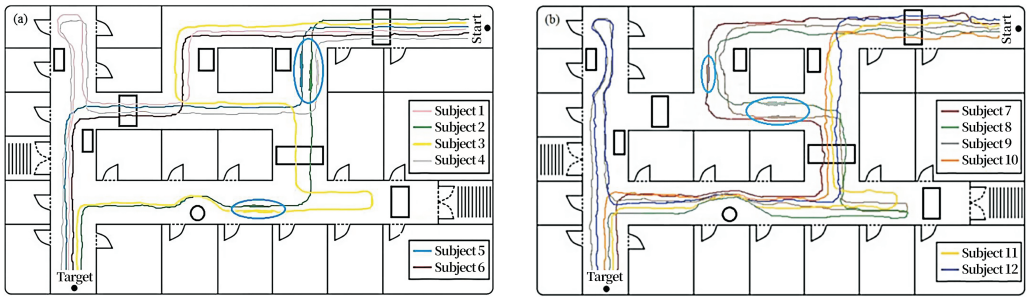

(a) Trajectories of subjects 1–6 (b) Trajectories of subjects 7–12

Fig. 1. Actual trajectories of subjects 1–12

rotation errors. Subjects 7–12 did not select all feasible flight directions (without executing MI tasks within 5 s). They must execute MI tasks to control UAV independently until next time feasible flight directions selection. Due to the short time adaptation, the second half of actual flight trajectories of subjects 7–12 were close to subjects 1–6. In the blue marked areas, the trajectories were relatively chaotic. The reason is that UAV automatically retreats and then flies forward to avoid people.

In Table 1, the distance and rotation errors of subjects 7–12 are about 1.5 times higher than those of subjects 1–6 and they use more time and MI tasks. The average time cost of subjects 7–12 is longer than that of subjects 1–6, about 110 s, and the average classification accuracy is reduced by about 12%. From another aspect, it can be inferred that subjects 7–12 can master how to use this BCI system in a short time and successfully complete actual indoor space target searching experiment. It verifies that this BCI system has good adaptability.

As shown in Table 2, subjects 7–12 did not choose the feasible flight direction in the first part. They had to execute MI tasks to control UAV independently. They took more time, had lower classification accuracy and produced larger distance and rotation errors. In the second part, subjects 7–12 basically mastered the MI tasks, so the classification accuracy was close to the average accuracy. The distance errors and rotation errors were significantly reduced. The distance errors and rotation errors of subjects 7–12 were reduced to 6.92 ± 1.9 – 7.46 ± 2.2 cm, and $7.21 \pm 2.0^\circ$ – $8.44 \pm 2.2^\circ$, respectively. The average distance errors decreased by about 5.32 cm and the average rotation error was reduced by about 5.86°. Subjects 7–12 mastered the four MI tasks quickly and the control accuracy of the second part was also close to subjects 1–6. It indicates that this BCI system has good adaptability.

Compared with other research, the average time for subjects 1–12 to realize the indoor target searching experiment was reduced by about 20 s [2]. The reason is that this BCI system replaces the interface switching subsystem with the feet and tongue MI tasks. However, the classification accuracy was reduced by about 21%. The main reason is that the four-classification difficulty and complexity are significantly greater than two-classification strategy. Since subjects only need to execute four kinds of MI tasks to select provided directions, it greatly reduces the burden of subjects.

Conclusion. This paper puts forward a BCI system to achieve indoor space target searching using a low speed UAV. It utilizes the SIFT algorithm and BF algorithm to extract key points and match the extracted feature points. To build the decision subsystem, the OVR and OVO strategies based on CSP and 2-layer HSVM method were employed to extract four kinds of MI tasks EEG features and complete the feature classification respectively. The actual indoor space target searching experiment verifies that this BCI system has good adaptability and stability. This BCI system directly implements 3D feasible flight direction selection

and only performs the MI tasks selecting feasible flight directions. It minimizes the burden of subjects and enables them to accomplish the control tasks for a long time.

REFERENCES

[1] Micheal A. A., K. Vani, S. Sanjeevi, C. Lin (2021) Object detection and tracking with UAV data using deep learning, J. India. Soc. Remote Sens., **49**, 463–469.

[2] Shi T., H. Wang, W. Cui, L. Ren (2019) Indoor space target searching based on EEG and EOG for UAV, Soft Comput., **23**, 11199–11215.

[3] Beg A., A. R. Qureshi, T. Sheltami, A. Yasar (2021) UAV-enabled intelligent traffic policing and emergency response handling system for the smart city, Person. Ubiq. Comput., **25**, 33–50.

[4] Simpson T. G., K. Rafferty (2021) Investigating the P300 response as a marker of working memory in virtual training environments, IEEE Trans. Hum. Mach. Syst., **51**(3), 265–277.

[5] Ojha M. K., M. K. Mukul (2021) A novel approach based on EMD to improve the performance of SSVEP based BCI system, Wireless Person. Commun., **118**, 2455–2467.

[6] Grigorev N. A., A. O. Savosenkov, M. V. Lukoyanov, A. Udoratina, N. N. Shusharina et al. (2021) A BCI-based vibrotactile neurofeedback training improves motor cortical excitability during motor imagery, IEEE Trans. Neur. Syst. Rehabilit. Eng., **29**, 1583–1592.

[7] Choi J. W., S. Huh, S. Jo (2020) Improving performance in motor imagery BCI-based control applications via virtually embodied feedback, Comput. Biol. Med., **127**, 104079.

[8] Zhang C., L. Sun, F. Cong, T. Ristaniemi (2021) Spatiotemporal dynamical analysis of brain activity during mental fatigue process, IEEE Trans. Cogn. Develop. Syst., **13**(3), 593–606.

[9] Benzy V. K., A. P. Vinod, R. Subasree, S. Alladi, K. Raghavendra (2020) Motor imagery hand movement direction decoding using brain computer interface to aid stroke recovery and rehabilitation, IEEE Trans. Neur. Syst. Rehabilit. Eng., **28**(12), 3051–3062.

[10] Häne C., L. Heng, G. H. Lee, F. Fraundorfer, P. Furgale, T. Sattler, M. Pollefeys (2017) 3D visual perception for self-driving cars using a multi-camera system: calibration, mapping, localization, and obstacle detection, Image Vision Comput., **68**, 14–27.

[11] Carrio A., Y. Lin, S. Saripalli, P. Campoy (2017) Obstacle detection system for small UAVs using ADS-B and thermal imaging, J. Intell. Robot. Syst., **88**(2–4), 583–595.

[12] Kwon J. W., J. Seo, J. H. Kim (2014) Multi-UAV-based stereo vision system without GPS for ground obstacle mapping to assist path planning of UGV, Electr. Lett., **50**(20), 1431–1432.

[13] Shi T. W., G. M. Chang, J. F. Qiang, L. Ren, W. H. Cui (2022) Brain computer interface system based on monocular vision and motor imagery for UAV indoor space target searching, Biomed. Signal Proc. Control, **79**, 104114.
[14] Dong E., C. Li, L. Li, S. Du, A. N. Belkacem, C. Chen (2017) Classification of multi-class motor imagery with a novel hierarchical SVM algorithm for brain–computer interfaces, Med. Biol. Eng. Comput., **55**, 1809–1818.

School of Computer Science
and Software Engineering
University of Science
and Technology Liaoning
114051 Anshan, Liaoning, China
e-mail: tianweiabbcc@163.com
176878392@qq.com
tianwei@ustl.edu.cn

School of Innovation
and Entrepreneurship
University of Science
and Technology Liaoning
114051, Anshan, China
e-mail: renlingqianzhihe@163.com